The Global Mapping of Mercury's Surface From SIMBIO-SYS Onboard BepiColombo: VIS-NIR Hyperspectral Coverage by the VIHI Channel

Gianrico Filacchione, Fabrizio Capaccioni, Emanuele Simioni, and Gabriele Cremonese

***Abstract*— One of the main goals of SIMBIO-SYS, the Spectrometer and Imagers for Mercury Planet Orbiter (MPO) BepiColombo (BC)-Integrated Observatory SYStem, on board ESA's BC mission is to image the entire surface of Mercury. During the first year of operations, the visible and infrared hyperspectral imager (VIHI), one of the three optical channels of SIMBIO-SYS, will be used in accordance with the scientific requirements of the mission, to build a global map of the planet in the spectral range 0.4–2.0 μm with a spectral sampling of 12.5 nm/band and a spatial resolution of 400 m/px. This map will be employed to derive mineralogy and surface regolith physical properties by means of spectrophotometric analyses. For the purpose of reaching this goal, a deterministic method able to predict the best GM strategy for VIHI in terms of time sequences, coverage, spatial sampling, integration/repetition times, signal-to-noise ratio (SNR) optimization, and data redundancy is discussed. Starting from these criteria, the determination of the timeline containing the sequence of the instrumental telecommands is derived from the orbital kernels of the spacecraft and within the limitation of the allocated data volume which poses strict operational constraints on the data generation and redundancy.**

***Index Terms*— Computational infrastructure and GIS, extraterrestrial sensing, hyperspectral data, miscellaneous applications, sensing platforms.**

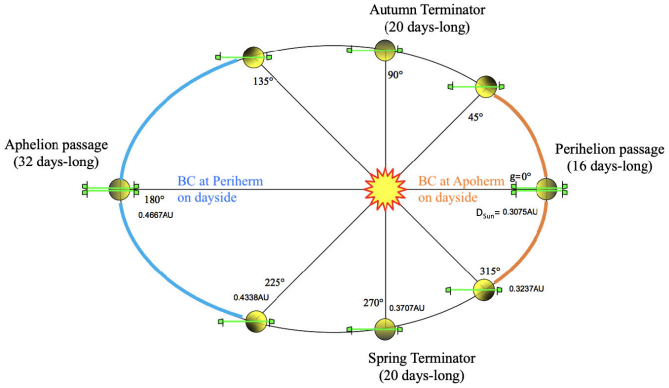

Fig. 1. Schematic of BC's (polar) orbits (green lines) and that of Mercury as seen from the Sun's north pole. When Mercury is at perihelion (TA = 0°) MPO is orbiting at apocenter (or apoherm, at 1500 km altitude) on the equator at dayside. Conversely, when Mercury is at aphelion (TA = 180°) MPO is at pericenter (or periherm, at 480 km) on the equator at dayside (the reverse on nightside). The boundaries of the four seasonal phases along the 88-days orbital period are indicated. Remote sensing observations will be performed preferentially during the perihelion (orange arc) and aphelion (blue arc) passages to achieve better solar illumination conditions.

I. Introduction

ESA'S BepiColombo (BC) spacecraft will be the first European mission designed to explore planet Mercury [1]. The mission was launched in 2018 with an Ariane 5 from Kourou spaceport (French Guyana) and will start orbital insertion at Mercury in December 2025 finishing by March 2026. BC consists of two modular orbiters, a Mercury Planet Orbiter (MPO) provided by ESA, and a Mercury Magnetospheric Orbiter (MIO) built by JAXA [2]. The two orbiters, stacked together at launch and during the cruise phase, are carried and placed in orbit around Mercury by the Mercury Transfer Module (MTM) which provides solar-electric and chemical propulsions. The MPO spacecraft will be inserted on an elliptical polar orbit around Mercury with an apocenter at 1500 km and a pericenter at 480 km altitude at the beginning of the mission which will progressively decrease down to 250 km (after 800 days). The nominal period of the initial orbit is 2.36 h. A schematic of the BC orbit characteristics during one Mercury, or hermean, year is shown in Fig. 1. The remote sensing observations of the hermean surface will be executed during the aphelion and perihelion orbital phases, corresponding, respectively, to Mean True Anomaly $135° \leq \text{MTA} \leq 225°$ and $315° \leq \text{MTA} \leq 45°$ during which the solar phase is $0° \leq g \leq 45°$. In Table I is listed the timing of the aphelion and perihelion orbital phases with the range of surface longitudes observable during each of them.

The major optical payload onboard MPO is SIMBIO-SYS, the Spectrometer and Imagers for MPO BC-Integrated Observatory SYStem [3] which is designed to achieve global, regional, and local mapping of the Mercury surface at high spatial resolution and in a wide spectral range.

SIMBIO-SYS employs three independent optical channels observing in parallel, each of them providing different data of the surface: 1) the high-resolution imaging channel (HRIC, [4]) will return high-resolution visible-color images (through 550, 750, 880 nm and panchromatic filters) of specific

Manuscript received 8 October 2022; revised 4 March 2023 and 20 May 2023; accepted 31 August 2023. Date of publication 7 September 2023; date of current version 28 September 2023. This work was supported by the Italian Space Agency (ASI) to the Istituto Nazionale di Astrofisica under Contract I/022/1070 and Contract 2017-47-H.0. *(Corresponding author: Gianrico Filacchione.)*

Gianrico Filacchione and Fabrizio Capaccioni are with INAF-IAPS, Istituto di Astrofisica e Planetologia Spaziali, Area di Ricerca di Tor Vergata, 00133 Rome, Italy (e-mail: gianrico.filacchione@inaf.it).

Emanuele Simioni and Gabriele Cremonese are with INAF-Padua Observatory, 35122 Padua, Italy.

Digital Object Identifier 10.1109/TGRS.2023.3312788

TABLE I

BC'S TIMING, ALTITUDE (AT APHELION/PERIHELION PASSAGES) AND LONGITUDINAL SURFACE COVERAGE AT THE EQUATOR. (*) THE FIRST PART OF APHELION #0 PASSAGE UNTIL 27MAR2026 SHALL BE DEVOTED TO INSTRUMENT COMMISSIONING AT MERCURY AND NOT USED FOR GM

Orbital Phase	Start time	End time	SPC Altitude (km)	Start Lon (deg)	End Lon (deg)
Aphelion #0(*)	21MAR2026	20APR2026	470	3.2	172.6
Perihelion #1	11MAY2026	26MAY2026	1529	-135.0	128.5
Aphelion #1	16JUN2026	16JUL2026	429	-157.6	-5.0
Perihelion #2	6AUG2026	21AUG2026	1570	38.6	-45.6
Aphelion #2	12SEP2026	12OCT2026	391	4.3	174.7
Perihelion #3	2NOV2026	17NOV2026	1605	-129.9	134.2
Aphelion #3	9DEC2026	8JAN2027	356	-176.0	-5.4

target areas corresponding to about 20% of Mercury's surface area at pixel scale $\leq$12 m/px; 2) the STereoscopic imaging Channel (STC, [5]) will acquire paired images, taken with an offset angle of $\pm$21.375° from nadir direction, necessary to retrieve the surface's global digital terrain model (DTM) using a panchromatic filter with a pixel scale $\leq$120 m/px and color images (420, 550, 750, 920 nm) for selected regions; and 3) the visible and infrared hyperspectral imager (VIHI, [6]) will observe the entire Mercury surface in the 0.4–2.0 μm spectral range with a maximum spectral sampling of 6.25 nm/band and a pixel scale $\leq$500 m/px with selected regions of interest observed at 120 m/px.

So far, the most comprehensive exploration of Mercury by a space mission has been achieved by NASA's MESSENGER which studied the planet from 2011 to 2015 [7]. The spacecraft was placed on a very elliptical orbit (200 by 15.000 km) with an inclination of 80° and a period of 12 h. Since the pericenter of the orbit was on latitude 60° the remote sensing instruments were obtaining much better coverage and resolution across the north hemisphere than on the south [8]. On board MESSENGER, the point spectrometer MASCS-VIRS [9] is comparable to VIHI for its scientific goals. MASCS has returned about 5 million reflectance spectra of Mercury surface in the Visible (300–1050 nm) and Near Infrared (850–1450 nm) spectral range, with a spectral sampling of 5 nm within a circular Field-Of-View (FOV) of 0.023°. These data were exploited to derive the hermean surface mineralogy at both global and regional scales [10]. Most of the planet was observed by MASCS at high solar phase angle between 78° and 102° due to thermal limitations of the MESSENGER spacecraft. The spatial coverage of the MASCS data is quite sparse due to the intrinsic limitation of the point spectrometer configuration: depending on the integration time, altitude, and slant angle to the surface, the size of the MASCS circular footprint is ranging between 0.1 km (cross-track) by 3 km (down-track) to $\geq$6 by 7 km resulting in an elliptical shape in the majority of the cases. Finally, the response of the Near Infrared spectral channel is characterized by poor signal-to-noise performances on many observation cases [10].

The BC mission has been designed to overcome many of the orbital limitations affecting the MESSENGER spacecraft. As shown in Fig. 1 its orbital parameters allow to observe the surface of Mercury from a less elliptic orbit compared to MESSENGER one. This will permit us to observe the entire surface of the planet with comparable resolution and coverage on both hemispheres. The low solar phase angle (between 0° and 45°) occurring during the orbits dedicated to the acquisition of the GM data will be optimal for remote sensing observations. Being an imaging spectrometer, SIMBIO-SYS/VIHI is capable to collect 256 contiguous and simultaneous spectra along its slit direction, resulting in an improvement of the spatial coverage and resolution with respect to the MASCS-VIRS point spectrometer. Other enhancements offered by VIHI are: 1) the larger spectral range which allows us to explore wavelengths between 1.4 and 2.0 μm previously unobserved by MASCS-VIRS and 2) the superior sensitivity given by the noise-equivalent spectral radiance (NESR) which is $\leq$0.01 W/(m^2 μm sr) at nominal temperature (detector at 220 K and optical head structure at 280 K) and integration time of 30 ms [11] corresponding to a factor $\times$50 better than 0.5 W/(m^2 μm sr) as estimated for MASCS-VIRS by [12] on the VIS spectral range for a minimum detector's temperature of 10 °C.

Starting from these conditions, there are all the makings of a great advancement in the exploration of Mercury surface composition thanks to SIMBIO-SYS/VIHI imaging spectrometer.

In this article, we describe the method developed to achieve a global mapping (GM) of Mercury's surface with SIMBIO-SYS/VIHI during the first year of the mission. In Section II, a description of the VIHI instrument, including restrictions due to operational modes is given. The GM strategy and implementation is detailed in Section III. The results of the coverage simulations during the first three aphelion orbital phases are discussed in Section IV. A discussion of the proposed observation strategy is in Section V. A companion paper by Simioni et al. [23] describes a similar strategy implemented to build the global DTM from SIMBIO-SYS/STC data.

II. VIHI INSTRUMENT

The VIHI instrument is a compact imaging spectrometer operating in pushbroom mode in the 0.4–2.0 μm spectral range capable of achieving a maximum spectral sampling of 6.25 nm/band (256 bands) with an Instantaneous FOV (IFOV) of 250 μrad/px and a FOV of 64 mrad (256 samples). Its optical design is based on a modified Schmidt telescope (entrance pupil 2.5 cm, focal length = 160 mm, f/6.4) joined to the entrance slit of a Littrow spectrometer. A 2-D HgCdTe detector (256 $\times$ 256 active pixels, 40 μm pitch, 2$\cdot$10^6 Me$^-$ full well, 14 bit digitalization), actively cooled at $T \leq 220$ K is used as focal plane. For comparison, the maximum surface temperature of the planet is $\geq$700 K. Over the active side of the detector is mounted a variable wedge filter to suppress spectral orders from the plane diffraction grating. The spectrometer is equipped with: 1) an internal calibration unit housed in

the entrance baffle capable of injecting, on demand, the flux emitted from a LED and a QTH lamp, further filtered by spectral filters, into the telescope pupil by means of a semitransparent window and collimating optics [13] and 2) an electromechanical shutter placed immediately before the spectrometer's entrance slit capable of blocking the light collected by the telescope with the aim of periodically measuring the detector's dark current and background. This contribution will be automatically removed from the collected signal by the onboard electronics for each given integration time and operational mode resulting in an optimization of the scientific signal data compression.

VIHI can be commanded to operate in different modes from high spatial-high spectral mode (unbinned) to combinations of nominal/low spatial/spectral resolution as reported in Table II. The unbinned mode will be used mainly for high-resolution acquisitions on target of interest, while the three binned modes will be employed during GM. Notably, the BINx2 mode is designed to provide an equivalent squared pixel of 500 μrad by summing the signals collected by two adjacent physical pixels on the instantaneous frame with the signals acquired by the same pixels on the successive acquisition. In the BINx4 mode the same process is applied to produce a 1000 μrad squared pixel by summing the signals collected by four adjacent physical pixels on the instantaneous frame and then summing the signals of the same pixels collected during the next three acquisitions (see schematics of the binning modes in Fig. 2).

In this way, a 500 $\times$ 500 or 1000 $\times$ 1000 μrad equivalent IFOV is built in time for the two cases while preserving the 64 mrad FOV and the 12.5 nm/band spectral sampling. At each spatial sample of the frame corresponds a spectrum made up to 256 (in NOBIN) or 128 (in BINx0, BINx2, and BINx4) spectral bands (see Table II). Further modes, including spatial windowing along the FOV or selective spectral editing, are not discussed here because they are not relevant to the GM phase.

The stream of data produced by VIHI is acquired and processed by the SIMBIO-SYS main electronics which provides the data formatting, compression, and time-stamping before transmitting data and telemetry packets to the S/C mass memory through the SpaceWire interface. Due to the high cadence of the data production and the limited downlink data rate during the GM observation phases, VIHI data will be transmitted with variable temporal delays, up to 6 months after their acquisition. The S/C mass memory allows us to safely store the data for prolonged periods of time and to transmit them to ESA's Estrack radio stations at the first useful occurrence. This solution has been studied and implemented to guarantee the continuity of the scientific observations even when Mercury is in superior conjunction or close to the Sun and the data downlink rate toward the Earth is null or very small.

A full description of the VIHI instrument is given in [3], [6], and [14] while summaries of the prelaunch calibration measurements are detailed in [15] and [16].

III. VIHI GM Strategy

By using ESA SPICE [17] kernels (meta-kernel for BC Dataset v281, file bc_plan_v281_20211112_001.tm), we have derived 25 geometric parameters, listed in Appendix Table IV, necessary for the projection of the VIHI boresight (B) and of the four corners (1-2-3-4) of the instantaneous slit (or FOV).

As the MPO orbit is elliptical, the distance from the surface varies continuously during the observational phase. However, since we cannot vary continuously the operational parameters due to the limitation in the number of telecommands that can be uploaded and executed by the spacecraft every day, VIHI has to be commanded through an observation strategy that uses the five following criteria to maximize the scientific return and to achieve complete coverage of the hermean surface with a spatial sampling of $\approx$400 m/px.

1) *Footprint Contiguity:* A minimum 10% overlapping must be guaranteed along-track direction between successive pixels.
2) *Integration Time:* It is kept smaller than the dwell time to avoid smearing.
3) *Spatial Resolution:* Among the possible modes listed in Table II, the one which best matches the 400 m/px requirement is selected.
4) *Signal-to-Noise Ratio (SNR):* As computed through the VIHI radiometric model [11], [16], must be maximized.
5) *Surface Coverage:* Dynamical switch on/off based on redundancy criteria to optimize coverage and minimize data volume.

The spatial resolution of 400 m/px during the GM phase has been defined within the list of the BC's scientific requirements. As a consequence of the spacecraft's orbital motion, the VIHI operational parameters need to be dynamically adjusted along the orbit by tuning their parameters according to the aforementioned criteria. Moreover, the instrument observation cycles are commanded on the basis of redundancy criteria (discussed later) to optimize the data volume return. Starting from these criteria, the VIHI timeline along each orbit has been broken up into a variable number of segments, each one characterized by fixed observation parameters. At each change of telecommands/operational mode, thus at the beginning of each segment, VIHI collects a dark frame (by closing the shutter) to be subtracted from the subsequent acquisitions. For this reason, at the beginning of each segment, there will be a gap in coverage of $\leq$5 km in length along track, corresponding to the time necessary to close the shutter, acquire the dark frame, and reopen the shutter. These operations have a duration of roughly 1 s. The resulting coverage gaps need to be filled during a successive passage of the spacecraft over the same areas.

The footprint contiguity and the integration time depend on the dwell time, e.g., the time necessary for the slit to drift by one IFOV

$$t_{\text{dwell}} = \frac{\text{IFOV} \cdot D}{v} \tag{1}$$

where D is the surface distance and v is the velocity of the boresight on the surface. The minimum 10% overlapping between consecutive slits has been included as a safe margin to avoid gaps in coverage. This value derives from best practices acquired from past experiences with similar imaging spectrometers [18], [19]. In order to avoid smearing during a single acquisition and preserve high spatial resolution, the

TABLE II
VIHI OPERATIONAL MODES

Operational Mode	Hi Spatial Hi Spectral	Hi Spatial Nom Spectral	Nom Spatial Nom Spectral	Low Spatial Nom Spectral
Format (S×B)	256×256	256×128	128×128	64×128
$\Delta\lambda$ (nm)	6.25	12.5	12.5	12.5
IFOV (μrad)	250	250	500	1000
Mode	NOBIN	BINx0	BINx2	BINx4
Data Volume (kbit/slit, uncompr)	917	458	230	115
Data Volume (kbit/slit, compr)	131	66	33	17

integration time t_{exp} is limited to $\leq t_{\text{dwell}}/4$. The contiguity of successive slits is guaranteed by commanding a repetition time t_{rep}, e.g., the time interval occurring between two successive acquisitions, given by

$$t_{\text{rep}} = t_{\text{exp}} + t_{\text{ro}} \tag{2}$$

where t_{ro} is the readout time, or the time necessary to read the entire VIHI focal plane (256 samples by 256 bands) from the proximity electronics. The t_{ro} is $\leq$20 ms and is constant for all VIHI operational modes (Table II) because spatial and spectral binnings are managed by the main electronics on the full resolution data. The t_{rep} is finely tuned in order to implement a small overlap ($\leq$10%) between successive acquisitions by anticipating the start of the successive acquisition. In this way it is possible to avoid gaps along the track direction.

The five criteria aforementioned allow us to establish an algorithm adapted to the VIHI operational modes and BC orbital characteristics which starting from SPICE kernels allows an autonomous planning of the GM campaign. To better illustrate the sequence of acquisitions used by VIHI in the two binning modes (BINx2 and BINx4, as defined in Table II), in Fig. 2 are shown the series of starting and final positions of the instrument's slits as projected on the surface of Mercury.

Apart from dynamical constraints, the integration time needs to be further checked with respect to the VIHI radiometric model in order to maximize the SNR without reaching the dynamical saturation of the detector. The VIHI radiometric model and the NESR, as derived from prelaunch measurements at operational thermal conditions, are, respectively, described in [11] and [16] and for the sake of brevity are not repeated here. The computation of the SNR and the saturation check are performed at a wavelength of 1 μm where the instrument responsivity is maximum (at this wavelength the instrument's signal will start to saturate if the integration time is too long).

The Average Mercury Terrain (AMT) surface reflectance is computed following the model proposed by [20] as an intimate mixture made of 75% labradorite and 25% enstatite with an average grain size of 30 μm and 0.1 wt% submicroscopic metallic iron distributed in the grain coating.

The Mercury's expected surface spectral radiance measured by VIHI at 1 μm, $R(1\ \mu\text{m}, \text{ZA}, \text{MTA})$, is given by

$$R(1\ \mu\text{m}, \text{SZA}, \text{MTA}) = \cos(\text{SZA}) \cdot r(1\ \mu\text{m}) \cdot \frac{\text{SI}(1\ \text{AU})}{\pi D_{\text{Sun}}^2} \tag{3}$$

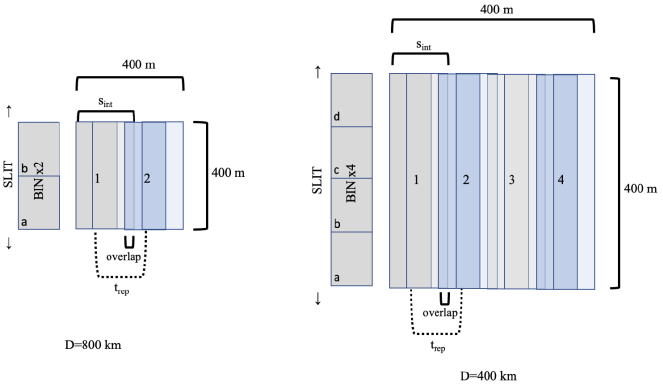

Fig. 2. Schematics of the acquisition of one VIHI spatial pixel in (left) BINx2 and (right) BINx4 modes. In gray color are shown the 2 (labels a, b) and 4 samples (labels a, b, c, d) along the slit which are binned together. In the BINx2 case two acquisitions are successively taken and the corresponding signals from the two pixels (a, b) are summed. For acquisition 1, it is shown that the projection of the starting IFOV (rendered in solid gray) and final IFOV (light gray) which moves in space due to the spacecraft's drift. The overall length of the projected slit along the track direction for an integration time (t_{exp}) is marked as s_{int}. Similarly for acquisition 2, in which the slit's starting and final positions are, respectively, marked in solid and light blue. The repetition time (t_{rep}), e.g., the time passing between the start of two consecutive acquisitions is computed by means of (2) and includes a prestarting to allow a 10 % spatial overlapping to guarantee contiguity. A similar scheme is shown for the BINx4 case (pixels a, b, c, d) for acquisitions 1–3 (in gray) and 2–4 (in blue). The 400 m spatial resolution is reached from a distance of 800 km in BINx2 and from 400 km in the BINx4 mode. The final signal transmitted on-ground in BINx2 and BINx4 modes is equal to the sum of 4 and 16 physical pixels, respectively.

where SZA, the solar zenith angle, is a function of the latitude observed at boresight (lat_B) and MTA along the orbit

$$\text{SZA} = \text{acos}(\cos(\text{lat}_B) \cdot \text{abs}(\cos(\pi - \text{MTA}))) \tag{4}$$

MTA being the Mercury True Anomaly (MTA), $r(1\ \mu\text{m})$ the AMT reflectance at 1 μm, equal to 0.24 from [20], SI is the Solar Irradiance (727 W/m^2/μm at 1 μm and at heliocentric distance of 1 AU,[1]) and D_{Sun} is the heliocentric distance of Mercury at the time of the simulation. Starting from the input radiance for a given position along the orbit, parametrized by means of Mercury's MTA and SZA, it is possible to simulate the VIHI signal in digital numbers (DNs) as

$$\text{DN}(1\ \mu\text{m}) = R(1\ \mu\text{m}, \text{SZA}, \text{MTA}) \cdot \text{Resp}(1\ \mu\text{m}) \cdot t_{\text{exp}} \tag{5}$$

where Resp(1 μm) is the average VIHI responsivity at wavelength of 1 μm equal to 1450 (DN m^2 μm sr)/(Ws)

[1]solar irradiance from http://rredc.nrel.gov/solar/spectra/am0/modtran.html

from [16]. Finally, the expected SNR is computed as

$$\mathrm{SNR}(1\ \mu\mathrm{m}) = \frac{\sqrt{\eta}\cdot \mathrm{DN}(1\ \mu\mathrm{m})}{\sqrt{\mathrm{DN}(1\ \mu\mathrm{m}) + \mathrm{DN}_{\mathrm{dark}}}} \tag{6}$$

where the instrument's dark current signal $\mathrm{DN}_{\mathrm{dark}}$, measured at the nominal detector's temperature (220 K), is parametrized as

$$\mathrm{DN}_{\mathrm{dark}} = 2160. + 40.29\cdot t_{\mathrm{exp}} \tag{7}$$

with t_{exp} the integration time in millisecond. In computing the SNR, the signal in DN needs to be converted in photoelectrons e^- by applying the instrument's transimpedence $\eta = 146\ e^-/\mathrm{DN}$.

The maximum signal threshold limit is fixed at 12 000 DN at 1 μm to avoid saturation, which occurs at 13 200 DN. This condition corresponds to an integration time of t_{exp}(12 000 DN, 1 μm). The integration time is therefore selected from the following condition:

$$t_{\mathrm{exp}} = \min\begin{cases} t(12\,000\mathrm{DN},\ 1\ \mu\mathrm{m}) \\ \dfrac{t_{\mathrm{dwell}}}{4}. \end{cases} \tag{8}$$

In view of the limited number of times it will be possible to change VIHI parameters during a given orbit, we will implement integration time changes only when the SNR becomes $\leq$100 along the orbit. To meet this requirement, the algorithm calculates the optimal integration time on the equator and then checks at each step north and southwards of it if the SNR $\geq$100 condition is kept. If the condition is not met, the integration time is increased until the SNR $\geq$100 condition is verified again. This method is applied independently on each hemisphere from the equator to the pole.

The surface coverage is the more demanding condition to be defined since it depends strictly on orbital parameters and needs to be finely tuned with respect to the mission scenario and operational constraints, such as data volume, spacecraft attitude, and thermal environment conditions. The current VIHI GM strategy has been defined for continuous observations acquired during the 32 days-long aphelion orbital arcs (135° $\leq$ TA $\leq$ 225°). Owing to Mercury's 3:2 orbital resonance and to BC's fixed orbital plane (see Fig. 1) it is possible to achieve complete coverage of the entire hermean surface by operating during the first three consecutive aphelion passages. The illumination conditions occurring during the observations are continuously varying because the solar phase steadily decreases from 45° at TA = 135° to 0° (opposition effect) at TA = 180° to increase again to 45° at TA = 225°. The ground track covers the southern to the northern pole, drifting toward negative longitudes on subsequent orbits. The VIHI switching on the criterion is based on the following conditions on the boresight longitude (lon_B) and on the maximum longitude covered by one of the slit's corner (lon_C):

$$\mathrm{lon}_B(k) \geq \mathrm{lon}_C(k+1) \tag{9}$$

$$\mathrm{lon}_B(k) \geq \mathrm{lon}_C(k+2) \tag{10}$$

$$\mathrm{lon}_B(k) \geq \mathrm{lon}_C(k+4) \tag{11}$$

$$\mathrm{lon}_B(k) \geq \mathrm{lon}_C(k+6). \tag{12}$$

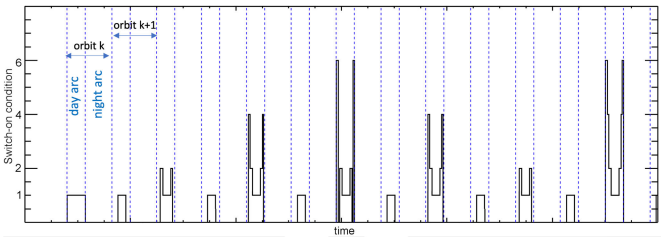

Fig. 3. Schematics of the switch-on/off timing along the first 13 orbits of aphelion #0 (TA = 135°). Y values 1, 2, 4, 6 correspond to conditions in (10)–(12), respectively.

The check is performed at each given latitude along the kth orbit with respect to the next orbits $k+1$, $k+2$, $k+4$, $k+6$th. The instrument is switched off if the projections of the slit on the surface overlap by more than 50% between successive orbits, while it is on if the overlap between the boresight and the slit corner is less than 50%. In Fig. 3 is shown that the time evolution of the switch on–off condition during the first 13 orbits occurring at the beginning of aphelion #0 (TA = 135°). VIHI will operate continuously during the first orbit k along the dayside arc and then is switched off once the spacecraft is over the nightside. On the next orbit $k+1$ the condition (10) will occur only in the equatorial part of the orbit where the instrument operates. At higher/lower latitudes the conditions (11)–(12) are not met and the instrument is off because the corresponding observed area has been already acquired during orbit k. Similarly, on orbit $k+2$ VIHI will be switched-on during a longer interval during which conditions (10) (at equator) and (11) (at low north and south latitudes) are met. Orbit $k+3$ is similar to $k+1$. In orbit $k+4$ are verified conditions (10)–(12) because the groundtrack evolution in longitude needs to be compensated by more extended coverage at higher latitudes. Condition (12) occurs typically every six orbits to guarantee the coverage of the polar regions.

Given the evolution of the orbital ground tracks, VIHI will make acquisitions in the equatorial region on each orbit. However, the instrument will not be operated as frequently over the polar regions, given the greater overlap in surface coverage and our operational constraints on the redundancy of surface coverage. As an example, during the equator passages during the aphelion #0 phase, the groundtrack is evolving in longitude by 0.6°/orbit corresponding to 25.5 km/orbit while the VIHI slit swath has a 30.2 km length. Therefore, according to (10), VIHI will be always on. Similar conditions will occur during the successive aphelions #1-#2 which will be necessary to complete the coverage. From aphelion #1 to aphelion #2, the width of the slit's projection on the surface drops from 27.6 to 25.0 km, respectively, while the groundtrack evolution remains fixed at 25.5 km/orbit at the equator. Around the middle of aphelion #2, the projections of the VIHI slit will drop to less than 25.0 km. This means that projected slits will be no more connected at equator since a gap of about 0.5 km will exist between consecutive orbits. This is a consequence of the evolution of the spacecraft's orbit, which reduces the altitude of the periherm at aphelion and increases the altitude of the apoherm at perihelion (see Table I), and it is the main

driver to accomplish the GM within the aphelion #2. While in principle it is possible to recover the gaps in coverage after aphelion #2, this operation will cost complex commanding of the instrument to minimize the additional data volume produced. Due to the limited data volume allocated to VIHI for achieving the GM, it is envisaged to complete it by the middle of aphelion #2.

IV. Coverage Simulations

In the following Sections IV-A–IV-C the resulting coverages achievable during Aphelions #0, #1, and #2 are discussed. The resulting total coverage from these three phases is discussed in Section IV-D where a calculation of the overall data volume and statistics on the operational modes established by the algorithm are given. In Figs. 4–14 are shown the maps with the most relevant quantities computed to achieve the GM and the corresponding range of longitudes as covered during the three aphelia passages.

A. Aphelion #0

The Aphelion #0 mapping phase starts when the spacecraft is orbiting above lon $\approx -45°$, encompasses the aphelion passage occurring at lon $= -90°$ and finishes at lon $= -180°$. In Fig. 4 is shown that the map of the MTA evolution during the dayside arcs of the Aphelion #0 (marked by the caption at the bottom of the figure). For convenience, the MTA evolution during successive aphelia passages is shown on the same map. All maps shown thereafter represent the VIHI slit as rendered in simple cylindrical projection using the standard hermean ellipsoid shape (without considering local topography). The coverage and position of the VIHI slit is computed through the algorithm described in Section III. The VIHI ground track evolves from south to north latitudes and toward more negative longitudes. The area of the surface rendered in deep orange-red color is observed before the Aphelion #0 passage (MTA $\leq -180°$) while the part in black-deep purple is covered after the aphelion (MTA $\geq 180°$). The small gap extending across 6 continuous orbits corresponding to longitude $-90°$ is artificial and due to the infeasibility of the criterion near the spacecraft's orientation flip, a maneuver necessary to maintain the spacecraft's cold radiator oriented along the anti-Sun direction. The gap will be filled during the planning once the last version of the ephemerides will be delivered.

The spacecraft-surface distance variations characterizing the Aphelion #0 phase are shown in Figs. 5 and 6. The minimum distance (464 km) will be reached in the range of latitudes from equator to lat $\approx 30°$ while the maximum (1045 km) will be reached above the south pole. For comparison, the spacecraft will orbit at about 750 km above the north pole. For the sake of brevity the polar maps shown in Fig. 6 are not repeated for all the remaining computed parameters.

The solar incidence angle during the Aphelion #0 orbital phase is shown in Fig. 7. The opposition effect regime (null incidence) is verified at equator during the aphelion passage (MTA $= 180°$, rendered in black-deep purple color). During this period of time the solar phase angle is null because the solar direction is parallel to the VIHI line of sight and the surface radiance is maximized. At equator, the incidence angle is equal to 180°-MTA while moving toward the polar regions it rapidly drops due to the ellipsoid surface's curvature.

The variability of the VIHI optimal repetition time (2) is given in Fig 8. The minimum repetition time (42 ms) is achieved between $0° \leq$ lat $\leq 20°$ while the maximum (137 ms) is reached on the south pole. The overall trend of the repetition

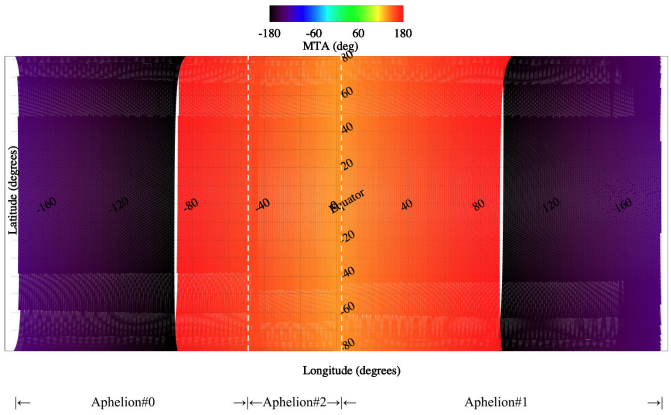

Fig. 4. Simple cylindrical projection map of the MTA evolution occurring during Aphelia #0-1-2 orbital phases. The range of longitudes covered during each aphelion phase is indicated in the legend at the bottom. The same scheme is repeated for the following cylindrical maps.

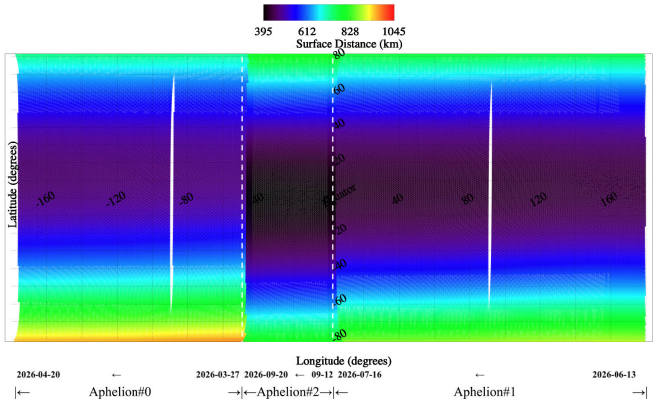

Fig. 5. Simple cylindrical projection of the spacecraft-surface distance evolution occurring during Aphelia #0-1-2 orbital phases. At the bottom are shown the start and end dates for each aphelion passage mapping phase. On each orbit the on-ground track moves from south to north latitudes.

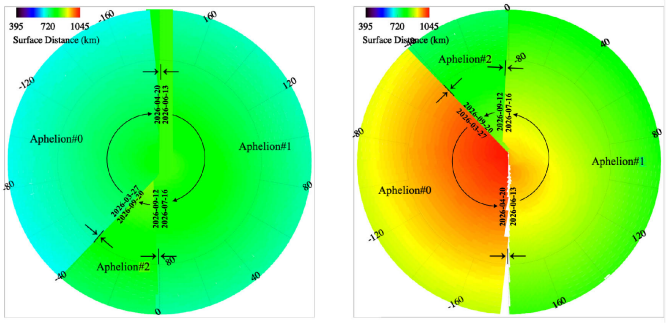

Fig. 6. Polar projection (left) north pole; (right) south pole of the spacecraft-surface distance evolution occurring during Aphelia #0-1-2 orbital phases. The small gap visible at longitude 180° on the south pole map is artificial and due to map rendering procedure. The start and end dates for each aphelion passage mapping phase are shown.

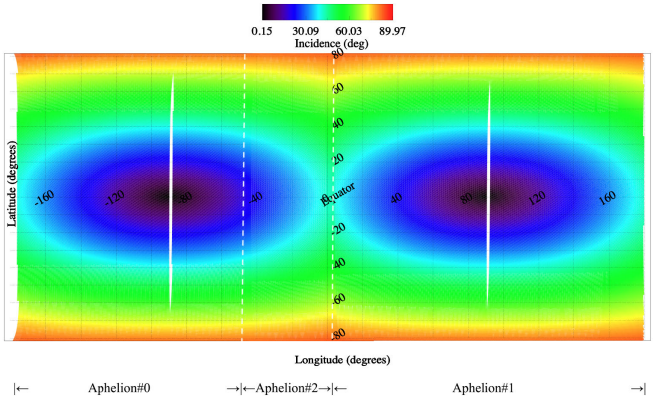

Fig. 7. Simple cylindrical projection of the incidence angle evolution occurring during Aphelia #0-1-2 orbital phases.

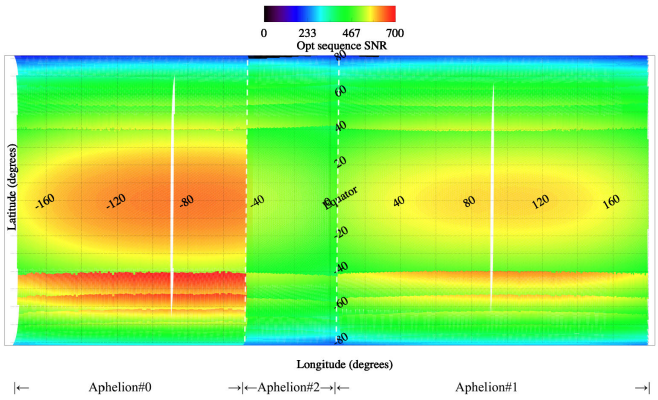

Fig. 10. Simple cylindrical projection of the VIHI SNR at 1 μm for Aphelia #0-1-2 orbital phases.

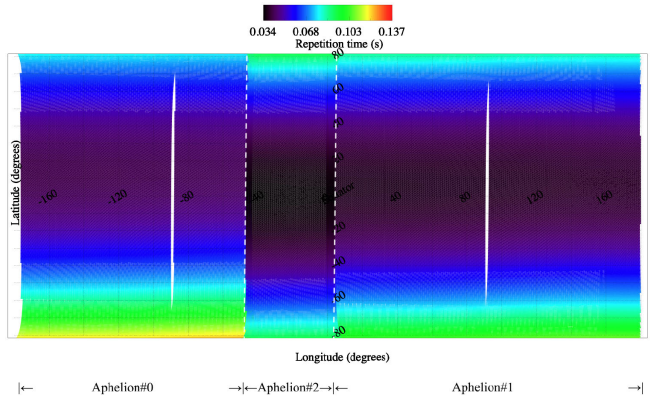

Fig. 8. Simple cylindrical projection of the VIHI optimal repetition time for Aphelia #0-1-2 orbital phases.

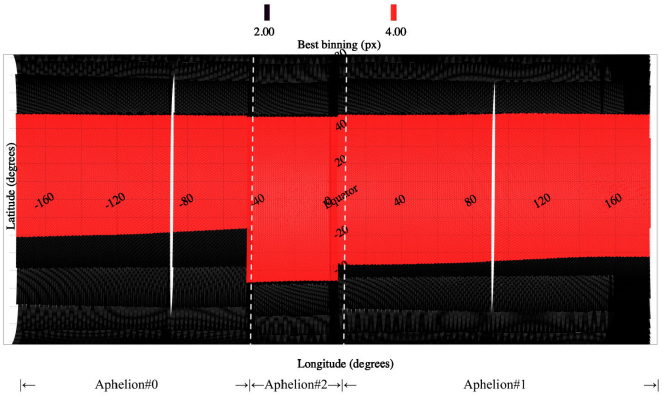

Fig. 11. Simple cylindrical projection of the VIHI optimal spatial binning mode for Aphelia #0-1-2 orbital phases.

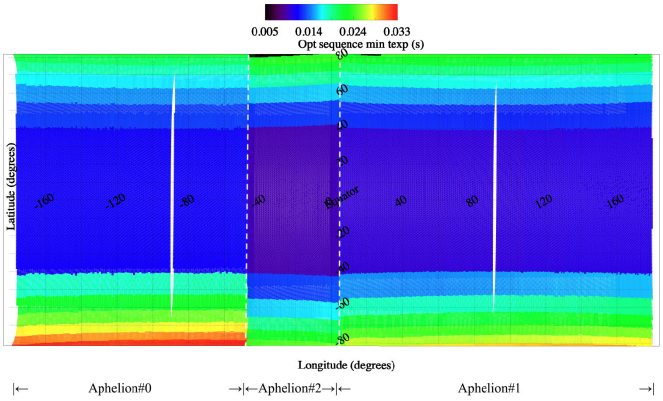

Fig. 9. Simple cylindrical projection of the VIHI optimal minimum integration time for Aphelia #0-1-2 orbital phases.

time follows the one of the spacecraft-surface distance shown previously in Fig. 5

Fig. 9 shows the minimum integration time as defined by the criterion given in (8). It ranges between 9 ms at the equator and 33 ms on the south pole. The integration time is optimized to reduce the number of telecommmands by maintaining the same value along a minimum number of orbital arcs during which the SNR $\leq$ 100.

Once the minimum integration time is defined it is possible to compute the corresponding signal (in DN) following (5) and then the SNR from (6). The map showing the SNR (1 μm) variation across the surface is shown in Fig. 10. The SNR distribution is modulated by the incidence angle and by the minimum integration time. The maximum SNR $\approx$700 is reached across the southern latitudes due to an optimal combination of incidence angle and integration time. On the equatorial regions, the SNR is about 600 while on the north polar region the SNR drops due to the very high incidence angle. One has to consider, however, that these values refer to spherical shape geometry and that in the real case, due to the surface roughness of Mercury's polar regions, the incidence angle could be much lower (for example, on illuminated craters rims) resulting in an improvement of the SNR.

Apart from the integration time, the overall number of operational sequences to be commanded during a given orbit is also a function of the spatial binning mode (Table II) which is selected to meet the 400 m/px requirement. In Fig. 11 are mapped the areas of the surface imaged with a spatial BINx2 (black color) and BINx4 (red color). The binning x2 is implemented toward the poles when the spacecraft-surface distance is higher while the binning x4 is systematically used on the equatorial to mid-latitudes where the distance is smaller.

As a consequence of the spacecraft-surface distance and binning mode, the resulting VIHI spatial resolution varies around the 400 m/pix requisite between 267 and 533 m/px. The best resolution is achieved on two longitudinal belts

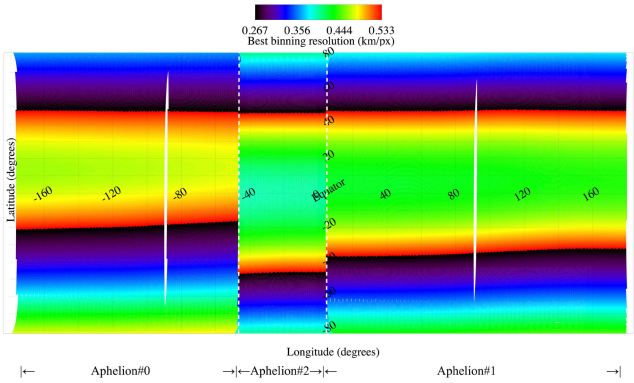

Fig. 12. Simple cylindrical projection of the VIHI spatial resolution for Aphelia #0-1-2 orbital phases.

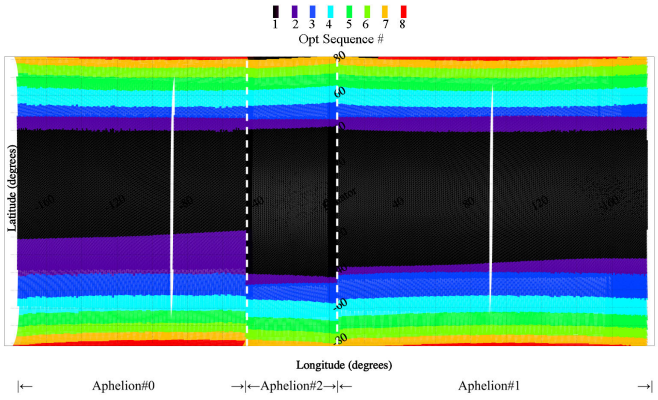

Fig. 13. Simple cylindrical projection of the number of VIHI operational sequences optimized for Aphelia #0-1-2 orbital phases.

running between latitudes −20° to −40° and 47° to 60°. The lower spatial resolution is reached on the two equatorward contiguous belts (Fig. 12). These values are the ones that best match the 400 m/px resolution requirement given the discretization of the VIHI operational modes and orbital parameters.

The merging of the two conditions about integration time (Fig. 9) and binning mode (Fig. 11) defines the total number of operational sequences, each of which is defined by a constant set of instrumental parameters (Fig. 13). For each orbit in Aphelion #0 the operational sequence characterized by the longest duration is the #1 (rendered in black color) centered on the equatorial belt. On each dayside orbital arc VIHI will change its operational mode for 15 times (one at the equator and seven on both the north and south hemispheres) to match the requirements listed in Section III. The scale of the map conceals the small gaps in coverage occurring at each change of the operational mode (between the boundaries of the regions rendered with different colors): these small gaps, approximately ≤5 km in length along the track direction, will be recovered during successive phases of the mission.

Finally, once the timing of the operational sequences is defined it is possible to compute the resulting data redundancy (Fig. 14) and data volume. The data redundancy map is rendered by adopting a regular grid of 400 × 400 m cells: the value shown for each cell corresponds to the number of times a

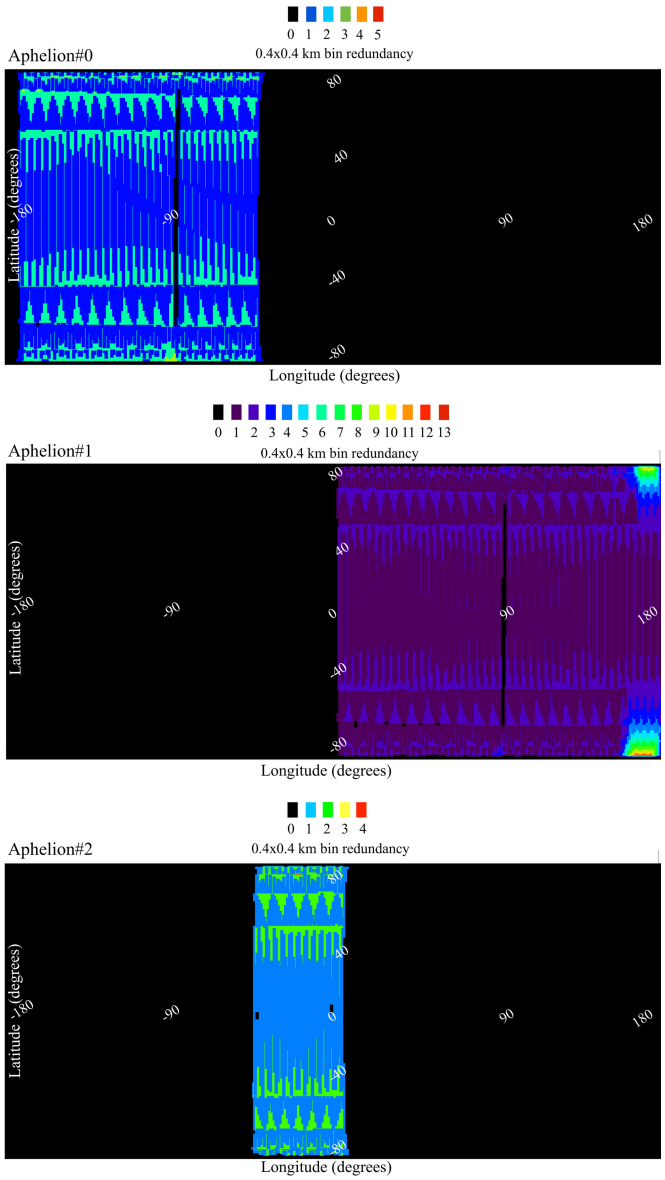

Fig. 14. Simple cylindrical projection of the GM data redundancy computed on a regular grid of 400 × 400 m cells during the (top panel) Aphelion #0, (center) Aphelion #1, and (bottom) Aphelion #2 orbital phases.

given VIHI slit is overlapping with it. A maximum redundancy by a factor ×5 is reached above the polar regions (not shown in the cylindrical projection map in Fig. 14). The majority of the surface rendered in blue color is acquired one time. The irregular patterns marked with cyan color have a redundancy factor of 2. As a result of the GM commanding strategy, the data volume generated by VIHI during the Aphelion#0 phase is 83 Gbits (compressed) as reported in Table III.

B. Aphelion #1

During the Aphelion #1 orbital phase (Table I) VIHI will map approximately the entire hemisphere between 0° ≤ lon ≤ 180 °. As a consequence of Mercury's and BC's orbital characteristics, the aphelion passage occurs on the meridian placed at lon = 90° with illumination conditions similar to the ones previously discussed for Aphelion #0. The

TABLE III
VIHI DATA VOLUME GENERATED DURING THE GM PHASE

	Aphelion#0	**Aphelion#1**	**Aphelion#2**	**Total**
Longitude range	-43° to -178.4°	179.6° to -2.7°	3.8° to -48.9°	full
Total Nr. of Spectra (px)	41.5E9	55.8E9	14.1E9	111.4E9
Nr. of Orbits	226	305	90	621
Nr. Frames BINx0	0	0	0	0
Nr. Frames BINx2	1.8E6	2.1E6	4.1E5	4.3E6
Nr. Frames BINx4	1.4E6	2.7E6	9.2E5	5.0E6
Data Volume (Gbit, uncompr.)	581	781	198	1560
Data Volume (Gbit, compr.)	83	111	28	222
Efficiency ($Gbit_{cmpr}/deg_{lon}$)	0.62	0.61	0.53	n.a.

only significant differences between the two aphelion passages are: 1) the steady reduction of the spacecraft's pericenter altitude from 470 (Aphelion #0) to 429 km (Aphelion #1) and 2) the inclination of the orbit toward the southern hemisphere. These changes, which imply a higher spatial resolution and smaller slit swath during Aphelion #1 with respect to the Aphelion #0 phase, are taken into account by the algorithm and compensated according to the requirements.

Following the same scheme used to describe the GM strategy during the Aphelion #0 phase, in Figs. 4–14 shown simple cylindrical maps of the observation parameters computed for Aphelion #1. Similar to the previously discussed Aphelion #0 maps, the small gap extending across six continuous orbits centered on lon = 90° is artificial and due to the spacecraft's orientation flip occurring at aphelion.

The variation of the MTA during Aphelion #1 is shown in Fig. 4. The spacecraft-surface distance ranges between 424 km at the equator to 966 km above the south pole (Fig. 5). The incidence angle is null above the equator over lon = 90° at MTA = 180° (Fig. 7). The optimized repetition and minimum integration times are shown in Figs. 8 and 9, respectively. The former varies between 37 ms at the equator and 121 ms on the south pole. The latter is set between 10 and 30 ms. The maximum SNR ≈ 600 is reached across southern latitudes and on the equatorial area observed during the opposition effect regime (Fig. 10). The maximum SNR during Aphelion #1 phase is smaller (by about 100) with respect to Aphelion #0 due to the shorter integration times caused by the closer orbits. The best-binning setting (Fig. 11) is similar to the one discussed during Aphelion #0, with BINx4 on the equatorial belt between $-35° \leq$ lat $\leq 40°$ and BINx2 elsewhere. The resulting spatial resolution shown in Fig. 12 is in general better than the one reached during Aphelion #0 thanks to the lower orbital distance: the best spatial resolution of 267 m/px is achieved at mid-latitudes, e.g., southwards of latitude −35° and northwards of latitude 45°, where the BINx2 mode is set (see Fig. 11). The worst resolution of 533 m/px corresponds to the north and south edges of the BINx4 mode. The algorithm is segmenting the dayside arcs of each orbit in 15 segments, like in Aphelion #0. Finally, the data redundancy map (Fig. 14) rendered on a 400 × 400 m grid shows high values (up to 13) in the polar regions around lon = 180° while on average the rest of the surface is observed for 1–2 times with a pattern similar to the one discussed for the Aphelion #0 case. The resulting data volume associated with the Aphelion #1 GM phase is 111 Gbits (uncompressed, see Table III).

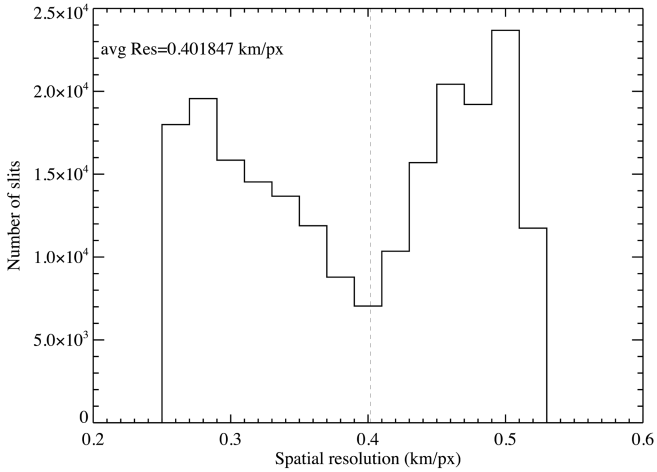

Fig. 15. Histogram of the spatial resolution achieved by VIHI during the GM. The average value (≈402 m/px) is indicated by the dashed line. The distribution is computed with a sampling of 20 m/bin.

C. Aphelion #2

To accomplish the full coverage of Mercury's surface in the current mission scenario, VIHI will need to operate through the final part of the Aphelion #2 phase (from 12 to 20 September 2026) to complete the coverage between longitude 3.8° and −48.9°, (see Table III) corresponding to the gap between Aphelion #0−#1 phases. In Figs. 4–14 are shown the simple cylindrical maps of the observation parameters computed for Aphelion #2 following the same scheme discussed previously.

During Aphelion #2, the MTA varies between 135° and 162° (Fig. 4). At this time the spacecraft-surface distance ranges between 395 km at the equator and 885 km in the polar regions (Fig. 5). The incidence angle is varying between 17.6° and 89.2° (Fig. 7). As shown in Fig. 8, the optimal repetition time is running between 34 ms at the equator and 105 ms on the polar regions. These values are a bit smaller than the similar ones derived during the previous aphelions due to the progressively lower altitude. The corresponding minimum integration time is 8 ms at the equator and up to 25 ms toward the poles (Fig. 9). The resulting SNR has a maximum value of about 550 on the equatorial belt (Fig. 10), smaller than the ones derived on the previous phases at the same latitudes due to the decrease of the integration time. The best binning solution (Fig. 11) and derived spatial resolution (Fig. 12) follow trends similar to the ones previously discussed. In general, due to

the evolution of BC's orbit periapsis toward southern latitudes, the best spatial resolution is reached at lower latitudes during Aphelion #2 than in the previous cases. The total number of sequences necessary to accomplish the computed coverage is 13 along a given orbit (Fig. 13). By implementing a similar observation strategy, VIHI will observe the area of Mercury's surface shown in (Fig. 14) with a data redundancy of 2 (regions in cyan color) and 3 (green color).

D. Total Coverage

As a result of the observation strategy previously discussed in Section III, VIHI will map the entire Mercury surface in 621 orbits distributed over the first three aphelion phases (Table III). The resulting onground spatial resolution will be between 267 and 533 m/px (Fig. 12). Due to the scale of the map, the gaps caused by the acquisition of the dark current frames each time VIHI will be commanded with a different set of instrument parameters are not shown. These gaps, $\leq$5 km in length along the track direction, will be filled during the successive phases of the mission when the subspacecraft's groundtrack will transit above them.

As summarized in Table III, to map the entire Mercury's surface VIHI will need to acquire more than 111 billion spectra corresponding to a data volume of 1560 Gbit (uncompressed) or 222 Gbit (compressed by a factor 7 by the onboard data compressor). Notably, the instrument will operate always in binned mode (BINx2, BINx4) to guarantee the 400 m/px scientific requirement and to remain within the data volume allocated at the mission level. Higher spatial resolution data, obtained in NOBIN and BINx0 modes (see Table II) will be dedicated to the observation of a specific target of interest, such as faculae and pyroplastic deposits [12], which will be observed by SIMBIO-SYS during the second year of the BC mission. The use of high-resolution modes for targets where higher spatial resolution is desired is under discussion within the team in the context of the target selection process [21].

V. Discussion and Conclusion

A deterministic method has been defined and tested to simulate the best GM strategy for VIHI in terms of time sequences, coverage, spatial sampling (converging to the 400 m/px requirement), integration/repetition times, SNR optimization, and data redundancy. Redundancy has been managed by checking coverage across multiple successive orbits with a discretization of 1, 2, 4, and 6 orbits. The method uses SPICE Kernels, as delivered by BC Science Ground Segment at ESA, to predict VIHI's slit position along orbits. The GM is built only during dayside arcs in Aphelia 0, 1, and 2 without using any Perihelion orbits. During the mapping phases, the spacecraft will be in quiet nadir pointing mode. Two reasons are behind the choice to operate only at apoherms: 1) the thermal environment of the spacecraft and consequently of VIHI will be worse at perihelion due to the lower heliocentric distance: this will cause an increase of the instrument thermal background and dark current with consequent degradation of the performances with respect to the aphelion case and 2) at periherm the ground tracks of consecutive orbits overlap much more, resulting in an inefficient mapping because a large portion of the slit is redundant: while at aphelion a data volume of about 0.53–0.61 Gbit (compressed) are necessary to map 1° in longitude from north to south, at perihelion the corresponding data volume would increase to $\geq$2 Gbit(compressed)/1 deg_{lon}. With the current GM strategy, the resulting data volume for VIHI is 222 Gbit (compressed) corresponding to 111 billion spectra. For comparison, as discussed in the Introduction, the MASCS spectrometer on MESSENGER has returned about 5 million spectra. VIHI will acquire >22 000 times more spectra than MASCS.

Our methodology can be validated thanks to the maps produced by the algorithm (Figs. 4–13) which show a uniform coverage of the surface by VIHI footprints without gaps in latitude between successive acquisitions. The footprints appear adequately connected also between consecutive orbits resulting in a regular coverage in longitude. The histogram of the spatial resolution achieved by VIHI during the GM campaign computed on the total number of slits (see Fig. 15) shows that the proposed strategy allows to reach an average spatial resolution of 402 m/px, a value which is matching the scientific requirement (400 m/px). The histogram has a bimodal dispersion showing two peaks at about 270 and 500 m/px which reflect the distribution of the spatial resolution shown on the map in Fig. 12. It is important to remark that the 400 m/px requirement refers to the average resolution for the GM as established in the mission scientific goals. Since the instrument has a discrete number of possible binning modes and the spacecraft is orbiting on an elliptical orbit, it is not possible to achieve a constant spatial resolution across the surface. Our results show that the average spatial resolution distribution across the GM is compliant with the scientific goal at the cost of mapping some areas with a spatial resolution as high as 533 m/px and others as low as 270 m/px.

Small adjustments and optimization of the starting-ending times of each mapping phase need to be implemented as soon as updated orbital kernels will be made available. A similar effort will be needed to define a strategy to recover the gaps due to operational mode changes and dark current acquisitions.

The GM optimization algorithm relies on the VIHI radiometric model derived from the prelaunch calibration campaign to compute the expected signal and SNR as a function of the illumination conditions and of the integration time assuming an average surface reflectance. For more specific cases, like for the study of ices in permanently shadowed polar areas [22], the integration time can be extended within the margins given by the dwell time.

Thanks to the algorithm developed to achieve the GM of Mercury's surface it will be possible to build a high resolution (400 m/px) hyperspectral map (0.4–2.0 μm) capable of tracing the hermean composition and surface regolith properties. The highly variable illumination conditions occurring during the aphelion passages, with solar phases running from 0° (opposition effect) to 45° will require a careful photometric correction to normalize the measured I/F to a common illumination geometry.

As discussed in a companion paper discussed in a companion (Simioni et al. [23]), while VIHI will be committed to the GM effort, Simbio-SYS/STC will acquire stereo color

TABLE IV
GEOMETRIC PARAMETERS USED FOR THE COMPUTATION AND OPTIMIZATION OF THE GM STRATEGY

Numeral	Parameter	Symbol	Units
1	EpochR time	ET	(hr)
2	Surface Distance	D	(km)
3	Latitude Boresight	lat_B	(deg)
4	Longitude Boresight	lon_B	(deg)
5	Mercury Radius at Boresight	R_B	(km)
6	Phase angle at Boresight	g	(deg)
7	Incidence angle at Boresight	i	(deg)
8	Emission angle Boresight	e	(deg)
9	Latitude corner 1	lat_1	(deg)
10	Longitude corner 1	lon_1	(deg)
11	Latitude corner 2	lat_2	(deg)
12	Longitude corner 2	lon_2	(deg)
13	Latitude corner 3	lat_3	(deg)
14	Longitude corner 3	lon_3	(deg)
15	Latitude corner 4	lat_4	(deg)
16	Longitude corner 4	lon_4	(deg)
17	Subnadir point latitude	lat_0	(deg)
18	Subnadir point longitude	lon_0	(deg)
19	Velocity of the Boresight	v_B	(km/s)
20	Velocity of the Boresight in Latitude	v_{B-lat}	(deg/s)
21	Swath angle along track	SA_{along}	(deg)
22	Swath angle across track	SA_{across}	(deg)
23	Subnadir point Distance	D_0	(km)
24	Heliocentric distance	D_{Sun}	(km)
25	Mean True Anomaly angle	MTA	(deg)

images to build the global DTM during the first year of the BC mission. In this way, for the first time, we will be able to perform a projection of hyperspectral/compositional data (from VIHI) and high-resolution images (from HRIC) over a digital elevation model (from STC) at the global scale. This effort will offer us a novel approach for the interpretation of remotely sensed data of a planetary surface.

Thanks to the intrinsic flexibility of the proposed algorithm, the SIMBIO-SYS operations team can rapidly reschedule the VIHI GM campaign in case of changes of the orbital scenario with respect to the nominal case: this is feasible because having established the five criteria aforementioned and the radiometric model, the determination of the timeline containing the sequence of the instrumental telecommands depends only from the orbital kernels of the spacecraft. Since pushbroom spectrometers rely on a similar concept of acquisition, the proposed algorithm, developed for the VIHI GM campaign at Mercury, through an appropriate tuning of the instrument's parameters and spacecraft kernels, could be scaled for any pushbroom imaging spectrometer aiming to map the entire surface of a spherical-shaped body.

APPENDIX

The list of the SPICE-computed geometric parameters used by the proposed algorithm for the computation and optimization of the GM strategy, including the determination the VIHI boresight and four corners of the FOV, are listed in the following Table IV.

ACKNOWLEDGMENT

The authors thank the three anonymous reviewers whose comments have contributed to improve the quality of the manuscript. They acknowledge technical support from BC's Mission Project team at ESA. This research has used NASA's Astrophysics Data System.

REFERENCES

[1] J. Benkhoff et al., "BepiColombo—Mission overview and science goals," *Space Sci. Rev.*, vol. 217, no. 8, p. 90, Dec. 2021.

[2] H. Hayakawa, Y. Kasaba, H. Yamakawa, H. Ogawa, and T. Mukai, "The BepiColombo/MMO model payload and operation plan," *Adv. Space Res.*, vol. 33, no. 12, pp. 2142–2146, Jan. 2004.

[3] G. Cremonese et al., "SIMBIO-SYS: Scientific cameras and spectrometer for the BepiColombo mission," *Space Sci. Rev.*, vol. 216, no. 5, p. 75, Jun. 2020.

[4] M. Zusi et al., "Optical design of the high resolution imaging channel of SIMBIO-SYS," *Appl. Opt.*, vol. 58, no. 15, p. 4059, May 2019.

[5] V. Da Deppo, G. Naletto, G. Cremonese, and L. Calamai, "Optical design of the single-detector planetary stereo camera for the BepiColombo European space agency mission to mercury," *Appl. Opt.*, vol. 49, no. 15, p. 2910, May 2010.

[6] F. Capaccioni et al., "VIS-NIR imaging spectroscopy of Mercury's surface: SIMBIO-SYS/VIHI experiment onboard the BepiColombo mission," *IEEE Trans. Geosci. Remote Sens.*, vol. 48, no. 11, pp. 3932–3940, Nov. 2010.

[7] S. C. Solomon et al., "The MESSENGER mission to mercury: Scientific objectives and implementation," *Planet. Space Sci.*, vol. 49, nos. 14–15, pp. 1445–1465, Dec. 2001.

[8] S. C. Solomon, R. L. McNutt, R. E. Gold, and D. L. Domingue, "MESSENGER mission overview," *Space Sci. Rev.*, vol. 131, nos. 1–4, pp. 3–39, Aug. 2007.

[9] W. E. McClintock and M. R. Lankton, "The mercury atmospheric and surface composition spectrometer for the MESSENGER mission," *Space Sci. Rev.*, vol. 131, nos. 1–4, pp. 481–521, Aug. 2007.

[10] N. R. Izenberg et al., "The low-iron, reduced surface of mercury as seen in spectral reflectance by MESSENGER," *Icarus*, vol. 228, pp. 364–374, Jan. 2014.

[11] G. Filacchione et al., "The measurement of the noise-equivalent spectral radiance of SIMBIO-SYS/VIHI spectrometer," in *Proc. 5th IEEE Int. Workshop Metrol. Aerosp. (MetroAeroSpace)*, Jun. 2018, pp. 252–256.

[12] A. Galiano, F. Capaccioni, G. Filacchione, and C. Carli, "Spectral identification of pyroclastic deposits on mercury with MASCS/MESSENGER data," *Icarus*, vol. 388, Dec. 2022, Art. no. 115233.

[13] F. Capaccioni et al., "Pre-launch calibrations of the Vis-IR hyperspectral imager (VIHI) onboard BepiColombo, the ESA mission to Mercury," *Proc. SPIE*, vol. 8867, Sep. 2013, Art. no. 886704.

[14] E. Flamini et al., "SIMBIO-SYS: The spectrometer and imagers integrated observatory system for the BepiColombo planetary orbiter," *Planet. Space Sci.*, vol. 58, nos. 1–2, pp. 125–143, Jan. 2010.

[15] F. Altieri et al., "The pre-launch characterization of SIMBIO-SYS/VIHI imaging spectrometer for the BepiColombo mission to Mercury. II. Spectral calibrations," *Rev. Sci. Instrum.*, vol. 88, no. 9, Sep. 2017, Art. no. 094503.

[16] G. Filacchione et al., "The pre-launch characterization of SIMBIO-SYS/VIHI imaging spectrometer for the BepiColombo mission to Mercury. I. Linearity, radiometry, and geometry calibrations," *Rev. Scientific Instrum.*, vol. 88, no. 9, Sep. 2017, Art. no. 094502.

[17] C. H. Acton, "Ancillary data services of NASA's navigation and ancillary information facility," *Planet. Space Sci.*, vol. 44, no. 1, pp. 65–70, Jan. 1996.

[18] A. Coradini et al., "VIRTIS: An imaging spectrometer for the Rosetta mission," *Space Sci. Rev.*, vol. 128, nos. 1–4, pp. 529–559, Feb. 2007.

[19] M. C. De Sanctis et al., "The VIR spectrometer," *Space Sci. Rev.*, vol. 163, nos. 1–4, pp. 329–369, Dec. 2011.

[20] J. Warell and D. T. Blewett, "Properties of the Hermean regolith: V. New optical reflectance spectra, comparison with lunar anorthosites, and mineralogical modelling," *Icarus*, vol. 168, no. 2, pp. 257–276, Apr. 2004.

[21] D. A. Rothery et al., "Rationale for BepiColombo studies of Mercury's surface and composition," *Space Sci. Rev.*, vol. 216, no. 4, p. 66, Jun. 2020.

[22] G. Filacchione et al., "Temporal evolution of the permanent shadowed regions at mercury poles: Applications for spectral detection of ices by SIMBIOSYS-VIHI on BepiColombo mission," *Monthly Notices Roy. Astronomical Soc.*, vol. 498, no. 1, pp. 1308–1318, Jul. 2020.

[23] E. Simioni et al., "The global mapping of Mercury's surface from SIMBIO-SYS onboard BepiColombo: 2) stereo coverage by the STC channel," submitted for publication.

Gianrico Filacchione received the master's degree in physics from La Sapienza University, Rome, Italy, in 2001, and the Ph.D. degree in aerospace engineering from Federico II University, Naples, Italy, in 2006.

He is currently a Researcher at INAF-IAPS, Rome. He has published more than 170 refereed manuscripts (H-index 48). His research interests range from VIS-IR imaging spectroscopy of planetary surfaces, including hyperspectral data analysis, observations planning and instrument calibration, to the development of new space instrumentation.

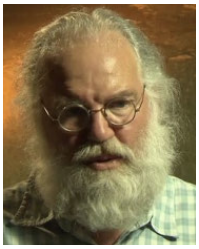

Fabrizio Capaccioni received the Ph.D. degree in physics from the Università La Sapienza, Rome, Italy, in 1982.

He is currently a Research Director at the "Istituto di Astrofisica e Planetologia Spaziali" (IAPS) of INAF, Rome. He is also a Co-Principal Investigator of the instrument SIMBIO-SYS onboard BepiColombo. His research interests comprise collisional fragmentation and evolution of asteroids, thermodynamical evolution of comets, participation to international space missions with the goal of study the surfaces of atmosphereless bodies by means of hyperspectral imaging instruments.

Emanuele Simioni is currently an Engineer at the Astronomical Observatory of Padova, INAF, Padua, Italy. He is also the Performance and Planning Manager of SIMBIO-SYS onboard BepiColombo and the responsible for the 3DPD reconstruction pipeline of the Padova Observatory currently in use for the DTMs generation of CaSSIS onboard ExoMars TGO. The main research topics are sensing image processing and passive and active 3-D reconstruction techniques, photogrammetry, and operations mainly for satellite stereo cameras.

Gabriele Cremonese has been an Astronomer at the Astronomical Observatory of Padova, INAF, Padua, Italy, since 1988. He is also the Principal Investigator of SIMBIO-SYS onboard BepiColombo and a Co-Principal Investigator of CaSSIS onboard ExoMars TGO. The main research topics are comets, planetary surfaces, exospheres, dynamical evolution of dust particles and space instruments, mainly cameras and stereo cameras.

Open Access funding provided by 'Istituto Nazionale di Astrofisica' within the CRUI CARE Agreement